2892 *Chem. Mater.* **2010,** *22,* 2892–2897
DOI:10.1021/cm100224b

CHEMISTRY OF MATERIALS
Article

Phase-Controlled Synthesis of Iron Silicide (Fe_3Si and $FeSi_2$) Nanoparticles in Solution

Naween Dahal and Viktor Chikan*

Department of Chemistry, Kansas State University, Manhattan, Kansas 66506-0401

Received January 24, 2010. Revised Manuscript Received March 14, 2010

In this study, a high-temperature reduction method is developed to prepare iron silicide nanoparticles in solution phase. The synthesis applies a reaction of silicon tetrachloride with iron pentacarbonyl in the presence of 1,2-hexadecanediol to form iron silicide nanoparticles. Under iron-rich synthetic conditions, superparamagnetic Fe_3Si nanoparticles form. The saturation magnetization of Fe_3Si nanoparticles has been found to be 60 emu/g by superconducting quantum interference device (SQUID) magnetometry technique. The value is close to that of iron oxide (Fe_3O_4) nanoparticles but less than that of iron nanoparticles. When silicon-rich conditions are used, mainly β-$FeSi_2$ nanoparticles form. The nanoparticle size, size distribution, and crystallinity are characterized by transmission electron microscopy (TEM), electron diffraction (ED), X-ray diffraction (XRD), and atomic force microscopy (AFM).

Introduction

As robust, stable, environmentally green, and inexpensive material,[1,2] iron silicides could take a critical role in the next generation of nanomaterials with a wide range of potential applications.[3] The bulk phase diagram of iron and silicon shows at least five known iron silicide compounds (Fe_3Si, Fe_5Si_3, FeSi, β-$FeSi_2$, and α-$FeSi_2$).[4] According to the phase diagram, ε-FeSi, β-$FeSi_2$, and Fe_3Si are stable at room temperature, whereas Fe_2Si, α-$FeSi_2$, and Fe_5Si_3 are metastable. These iron silicides exhibit metallic, semiconductor, or insulating behavior depending on their structure. Ferromagnetic properties are observed in iron-rich phases Fe_3Si and Fe_5Si_3.[5−8] FeSi acts as a Kondo insulators with increasing conductivity as a function of temeparture,[9,10] β-$FeSi_2$ is a narrow band gap (0.85 eV) semiconductor and potential photovoltaic material.[11,12] α-$FeSi_2$ is a metal and a potentially beneficial interface for silicon-based solar cells.[13] Fe_3Si is a good candidate as a ferromagnetic electrode in spintronics devices such as magnetic tunnel junctions.[7,14] The use of conventional ferromagnetic materials such as Fe or Co, suffers from oxidation and impedance mismatch between the ferromagnetic film and semiconductor. Fe_3Si has been proposed as an excellent alternative for those conventional materials.[15] Fe_3Si has a high Curie temperature of ~800 K, is oxidation resistant, and has a similar spin polarization to that of Fe and Co (45% in thin film) and a relatively high value of saturation magnetization (84 to 196 emu/g).[6,14,16] At room temperature, Fe_3Si crystallizes in the $D0_3$ crystal structure. The crystal structure is derived based on space group *Fm*3*m* and cubic unit-cell dimension of magnitude 5.665 Å.

Despite the interesting properties and potential applications, iron silicide is challenging to produce in a solution. Although gas-phase synthetic methods are described in the literature, no colloidal synthetic methods exist to produce such nanoparticles. There are some examples of self-assembled epitaxial thin films of Fe_3Si on Si, Ge, and

*Corresponding author.

(1) Zichichi, A., *Silicides Fundamentals and Applications*; World scientific Publishing: Singapore, 2000.
(2) Borisenko, V. E. *Semiconducting Silicides*; Springer: Berlin, 2000; p 39.
(3) Hafner, J.; Spisak, D. *Phys. Rev. B* **2007**, *75* (19), 195411.
(4) Hansen, M.; Anderko, K. *Constitution of Binary Alloys*., 2nd ed.; McGraw-Hill: New York, 1958; p 713.
(5) Kolel-Veetil, M. K.; Qadri, S. B.; Osofsky, M.; Goswami, R.; Keller, T. M. *J. Phys. Chem. C* **2009**, *113*(33), 14663–14671.
(6) Hamaya, K.; Ueda, K.; Kishi, Y.; Ando, Y.; Sadoh, T.; Miyao, M. *Appl. Phys. Lett.* **2008**, *93* (13).
(7) Mantovan, R.; Georgieva, M.; Fanciulli, M.; Goikhman, A.; Barantcev, N.; Lebedinskii, Y.; Zenkevich, A. *Phys. Status Solidi A* **2008**, *205*(8), 1753–1757.
(8) Jing, Y.; Xu, Y. H.; Wang, J. P. *J. Appl. Phys.* **2009**, *105* (7), B520.
(9) Schmitt, A. L.; Bierman, M. J.; Schmeisser, D.; Himpsel, F. J.; Jin, S. *Nano Lett.* **2006**, *6*, 1617.
(10) Fu, C.; Krijn, M.; Doniach, S. *Phys. Rev. B* **1994**, *49*(3), 2219–2222.
(11) Filonov, A. B.; Migas, D. B.; Shaposhnikov, V. L.; Dorozhkin, N. N.; Petrov, G. V.; Borisenko, V. E.; Henrion, W.; Lange, H. *J. Appl. Phys.* **1996**, *79*(10), 7708–7712.
(12) Antonov, V. N.; Jepsen, O.; Henrion, W.; Rebien, M.; Stauss, P.; Lange, H. *Phys. Rev. B* **1998**, *57*(15), 8934–8938.
(13) Kulatov, E.; Nakayama, H.; Ohta, H. *J. Phys. Soc. Jpn.* **2001**, *70* (7), 2199–2204.
(14) Ionescu, A.; Vaz, C. A. F.; Trypiniotis, T.; Gürtler, C. M.; García-Miquel, H.; Bland, J. A. C.; Vickers, M. E.; Dalgliesh, R. M.; Langridge, S.; Bugoslavsky, Y.; Miyoshi, Y.; Cohen, L. F.; Ziebeck, K. R. A. *Phys. Rev. B* **2005**, *71*(9), 094401.
(15) Min, B.-C.; Motohashi, K.; Lodder, C.; Jansen, R. *Nat. Mater.* **2006**, *5*(10), 817–822.
(16) Deneke, C.; Schumann, J.; Engelhard, R.; Thomas, J.; Muller, C.; Khatri, M. S.; Malachias, A.; Weisser, M.; Metzger, T. H.; Schmidt, O. G. *Nanotechnology* **2009**, *20* (4), 045703.
(17) Ando, Y.; Hamaya, K.; Kasahara, K.; Ueda, K.; Nozaki, Y.; Sadoh, T.; Maeda, Y.; Matsuyama, K.; Miyao, M. *J. Appl. Phys.* **2009**, *105* (7), B102.
(18) Liew, S. L.; Seng, D. H. L.; Tan, H. R.; Chi, D. Z. *J. Phys. D, Appl. Phys.* **2009**, *42* (10), 105006.
(19) Starke, U.; Weiss, W.; Kutschera, M.; Bandorf, R.; Heinz, K. *J. Appl. Phys.* **2002**, *91*(9), 6154–6161.

Published on Web 04/07/2010

GaAs substrates.[8,16−22] However, these examples are difficult to implement for many of the intended applications. The preparation of heuslar Fe_3Si nanoparticles by magnetron sputtering is also described in the literature.[8] There are recent reports of the synthesis of either FeSi nanowires from a single-source precursor molecule[9] or the preparation of Fe_5Si_3 nanowire and nanoparticles.[5,23]

The synthesis of nanoparticles from bulk iron silicide is challenging because of complex phase behavior and multiple stoichiometries of the material. Typically, iron silicides are produced at very high temperatures that are difficult to implement in solution. The stoichiometric composition of silicide can not be explained by a simple sets of rules based on oxidation state and electronegativity.[1] A key question is what phase of iron silicide would be produced if chemical reactions were carried out with or without stoichiometric control. This letter shows that it is possible to form highly crystalline iron silicide nanoparticles in solution with some phase and size control. In this particular method, iron pentacarbonyl and silicon tetrachloride are used as precursor molecules to produce iron silicide. From these precursor molecules, Fe_3Si or β-$FeSi_2$ is formed at relatively low temperatures.

Experimental Details

Chemicals. Iron pentacarbonyl $Fe(CO)_5$ 99.5% and silicon tetrachloride ($SiCl_4$) 99.99% were purchased from Strem chemicals. 1,2-Hexadecanediol techn. 90%, oleic acid 90%, triphenylphophine 90%, ethanol 95%, 1,2-dichlorobenzene 99%, and octyl ether 99% were purchased from Aldrich. All the chemicals are used as-received without further purification.

Synthesis of Fe_3Si Nanoparticles. Fe_3Si nanoparticles 4−7 nm in size are synthesized in a three-necked flask. In a typical synthesis, 20 mL of *o*-1,2-dichlorobenene or octyl ether is mixed with 4 mmol (1.03 g) of 1,2-hexadecanediol and heated to ∼220−250 °C. When *o*-1,2-dichlorobenzene is used as solvent, the mixture is heated to 180 °C. The solution is stirred for 10 min under an argon atmosphere. Following the dissolution of 1,2-hexadecanediol, 2 mmol (0.56 g) of oleic acid and 2 mmol (0.52 g) of triphenylphosphine are injected in the solution stepwise. Before the addition of triphenylphosphine, it is dissolved in 2 mL of either octyl ether or 1,2-dichlorobenzene and oleic is injected as received because it is liquid at room temperature. At this point of the synthesis, 20 mmol (3.91 g) of iron pentacarbonyl is added and the decomposition of iron pentacarbonyl results in the formation of iron nanoparticles. Immediately, the initial yellow solution changes to black as nanoparticle form. Within 10 s of iron pentacarbonyl injection, 6.6 mmol (1.12 g) of silicon tetrachloride is injected into the solution that leads to the formation of iron silicide nanoparticles. A vigorous reaction takes place forming dense fumes inside the condenser. (Extreme care should be taken while handling iron pentacarbonyl and 1,2-dichlorobenzene as both are toxic and inflammable.) The solution is refluxed under argon for 10−240 min. After injection of the silicon tetrachloride, the appearance of the solution changes from dense black to light black. When the stoichiometric ratio of silicon and iron is changed to 2:1, mostly β-$FeSi_2$ nanoparticles are formed. Interestingly, the iron monosilicide never forms under the experimental conditions, even when the ratio is changed to 1:1, but the reaction rather leads to the formation of Fe_3Si phase. The Fe_3Si nanoparticles synthesized in 1,2-dichlorobenzene are readily soluble in heptane or hexane.

Purification. The solution is cooled to room temperature after refluxing for 3 h, and 95% ethanol is added in excess and centrifuged for 10 min at 8500 rpm. The black brown precipitate is separated from the very light brown supernatant. The precipitate is dried and characterized by XRD. For further characterization, the precipitate is redissolved in hexane, followed by ultrasonic treatment for an hour in the presence of 0.8 mmol of oleic acid and 0.8 mmol of triphenylphosphine. The additions of ligands in this part of experiment help to increase the solubility of the nanoparticles. The solution is treated with excess ethanol (50 mL) to precipitate nanoparticles. The sample is centrifuged again at 8500 rpm for 10 min. Finally, the precipitate obtained is dissolved in hexane or heptane. This final solution is used to prepare samples for further characterizations.

Results and Discussion

Figure 1 shows powder X-ray diffraction (XRD) patterns of the Fe_3Si nanoparticles under different experimental conditions along with the calculated Fe_3Si X-ray diffraction peaks. The powder X-ray diffraction pattern reveals that the samples are homogeneous and crystalline. The XRD peaks at 27.30, 31.48, 45.30, 54.11, 56.28, 66.10, 75.14, and 83.76 2θ correspond to (111), (200), (220), (311), (222), (400), (420), and (422) lattice planes of $D0_3$ structure Fe_3Si nanoparticles. When iron rich conditions are used, experiments are carried out for 10−240 min refluxing time to assess the effect of refluxing time on the crystallinity and homogeneity of the samples. As Figure 1a clearly shows, the crystallinity and homogeneity of the samples are increased with longer refluxing times. Fe_3Si Nanoparticles that are obtained from refluxing longer time (240 min) visually show sharp peaks. However, when the peaks are fitted with Debye−Scherrer formula[24] to extract approximate particle size, the data confirmed that the crystallite sizes remain the same (∼8.5 ± 1.8 nm) as shown in Table 1. The most intense (200) peak is Gaussian fitted to data in each experiment and determines the width and the peak values as well as errors in these values from the Gaussian function. The result indicates that once the growth of the nanoparticles is taken place, monomer exchange among the particles is minimal. Interestingly, a small change in 2θ angles is observed in XRD patterns between the calculated (Figure 1a (V)) and the experimental results of the Fe_3Si nanoparticles. The small change in 2θ angles is attributed to the formation of thin sublayer of iron silicide (Fe_3Si) or silicon oxide that produce different residual strain on the nanoparticles. Similar behavior is reported

(20) Takeda, K.; Yoshitake, T.; Sakamoto, Y.; Hara, D.; Itakura, M.; Kuwano, N.; Nagayama, K. *Int. J. Mod. Phys. B* **2009**, *23*(17), 3543–3549.
(21) Schütte, M.; Wartchow, R.; Binnewies, M. *Z. Anorg. Allg. Chem.* **2003**, *629*(10), 1846–1850.
(22) Zhang, S. L.; Ostling, M. *Crit. Rev. Solid State Mater. Sci.* **2003**, *28*, 1.
(23) Varadwaj, K. S. K.; Seo, K.; In, J.; Mohanty, P.; Park, J.; Kim, B. *J. Am. Chem. Soc.* **2007**, *129*(27), 8594–8599.
(24) Dahal, N.; Chikan, V.; Jasinski, J.; Leppert, V. J. *Chem. Mater.* **2008**, *20*(20), 6389–6395.

in case of anatase (TiO_2), silver, and iron platinum nanoparticles.[25−27]

Stability and the robustness of the Fe_3Si nanoparticles are evaluated by annealing the nanoparticles at 500 to 900 °C in air. For comparison, the calculated XRD patterns of α-$Fesi_2$ and β-$FeSi_2$ are also presented in Figure 1b (I) & (II) respectively. When the nanoparticles are annealed below 450 °C, no change in the XRD pattern is observed (not shown in figure). However, when the nanoparticles are heated in air above 450 °C, phase change takes place in the material as shown in Figure 1b (III−V). When the nanoparticles are further heated (above 600 °C), the major peaks of Fe_3Si phase partially collapse as depicted in Figure 1b (V). Even further heating the nanoparticles to 700 °C results in the formation of the mixed phase of α-$FeSi_2$, β-$FeSi_2$, and Fe_5Si_3 (IV).[12,28,29] When the nanoparticles are heated to 900 °C, they exhibit the same phase as in 700 °C, but sharpening and narrowing of the XRD peaks is observed because of annealing (III). This is different from the bulk phase diagram of iron and silicon where Fe_5Si_3 is the expected product to be obtained upon annealing in the iron rich samples. When the XRD patterns of annealed sample at 900 °C is compared with calculated XRD patterns of Fe_5Si_3 and α-$FeSi_2$, the latter appears more prominent along with β-$FeSi_2$ (see the Supporting Information, Figure S1). The XRD peaks at 2θ degree 28.04 and 33.40 are the peak associated with Fe_5Si_3. During annealing, the absence of silicon dioxide peaks or iron oxide peaks (which are prone to form even at lower temperature) indicate that there is no phase segregation of the elements within the nanoparticles.

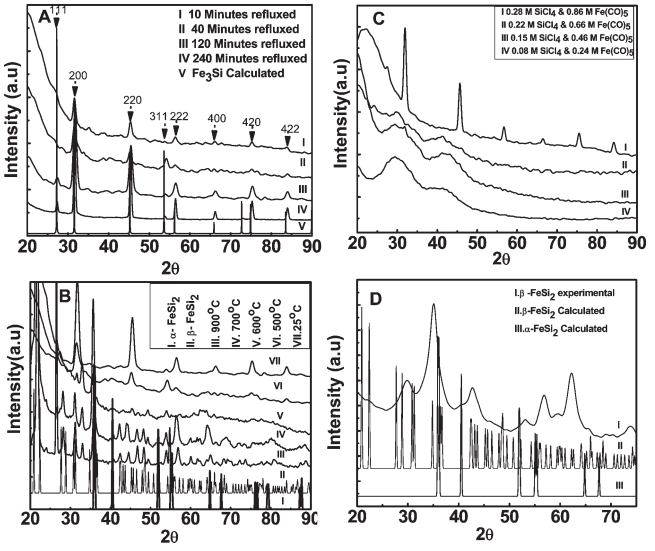

Figure 1. (A) XRD patterns of Fe_3Si nanoparticles prepared under different refluxing times: (I) 10, (II) 40, (III) 120, and (IV) 240 min, and calculated XRD patterns based on space group No. 225 and lattice constant 5.665 Å. (B) Calculated XRD patterns of α-$FeSi_2$ and β-$FeSi_2$ (I) and (II). XRD patterns of Fe_3Si nanoparticles annealed at different temperatures: (III) 900, (IV) 700, (V) 600, and (VI) 500 °C, and (VII) room temperature. (C) XRD patterns of Fe_3Si nanoparticles at different molar concentrations but a fixed molar ratio (3:1) of iron to silicon precursor: (I) 0.86 M iron to 0.28 M silicon precursor, (II) 0.66 M iron to 0.22 M silicon precursor, (III) 0.46 M iron to 0.15 M silicon precursor, and (IV) 0.24 M iron to 0.08 M silicon precursor. (D) XRD patterns of (I) β-$FeSi_2$ nanoparticles prepared from 1:2 molar ratios of iron to silicon precursor molecules, and (II) calculated XRD patterns of β-$FeSi_2$ and α-$FeSi_2$ based on their crystal geometries, lattice constants, and space groups.

Unusually, Fe_3Si nanoparticles are not formed in all concentrations of precursor molecules. as shown in Figure 1c. Several experiments are carried out at different concentrations of iron to silicon precursor molecules, keeping all variables in the reactions constant. When the concentration of iron to silicon precursors is 0.24 and 0.08 M, the reaction simply forms an amorphous material with broad atomic reflections at 30 and 40° 2θ as shown in Figure 1c (IV). Further increasing the concentration of iron to silicon precursor molecules from 0.46 and 0.15 M (this composition is later called the small Fe_3Si nanoparticles in this manuscript) to 0.66 to 0.22 M, the X-ray diffraction patterns do not show significant improvement in the crystallinity and homogeneity of the nanoparticles (Figure 1c III and II). The poor crystallinity and homogeneity in all concentrations except 0.86 M of iron precursor to 0.28 M of silicon precursor is probably due to very small cluster size and absence of favorable nucleation sites for formation of the nanoparticles. Crystalline Fe_3Si nanoparticles are formed in all experiments containing the iron to silicon precursors concentrations above or equal to 0.86 to 0.28 M as shown in Figure 1c (I) (nanoparticles for this composition are considered as large Fe_3Si nanoparticles in this manuscript). The effect of different reducing agents is also addressed in the synthesis of the Fe_3Si nanoparticles. In this particular experiment, 1,2-hexadecanediol is found to be the best reducer to produce crystalline iron silicide nanoparticles. Other reducers such as lithium−aluminum hydride, lithium triethylborohydride, and ethylene glycol simply cause the formation of amorphous material.

When the mole ratio of precursor molecules is 1:2 for iron to silicon, mainly β-$FeSi_2$ is formed (Figure 1d (I)).[30−32] Figure 1d (II) and (III) represents the calculated XRD patterns of β-$FeSi_2$ and α-$FeSi_2$ nanoparticles based on their orthorhombic and tetragonal crystal structures, lattice parameters, and crystallographic space groups. The close agreement of the experimental and calculated XRD pattern suggests the formation of β-$FeSi_2$ nanoparticles.

Figure 2a shows the low-magnification transmission electron microscope (TEM) image of the large Fe_3Si nanoparticles. The particles are prepared by taking 0.86 M iron

Table 1. Size Measurements of Fe_3Si and β-$FeSi_2$ nanoparticles from TEM, AFM, and XRD

		TEM		AFM		XRD	
S.N	samples	diameter (nm)	standard deviation	height (nm)	standard deviation	size (nm)	standard deviation
1	large Fe_3Si	7.5	±2.8	6.9	±1.5	8.5	±1.8
2	small Fe_3Si	4.2	±1.2	3.8	±1.0	5.3	±2.1
3	β-$FeSi_2$	9.6	±2.2	9.1	±3.5	12.4	±1.6

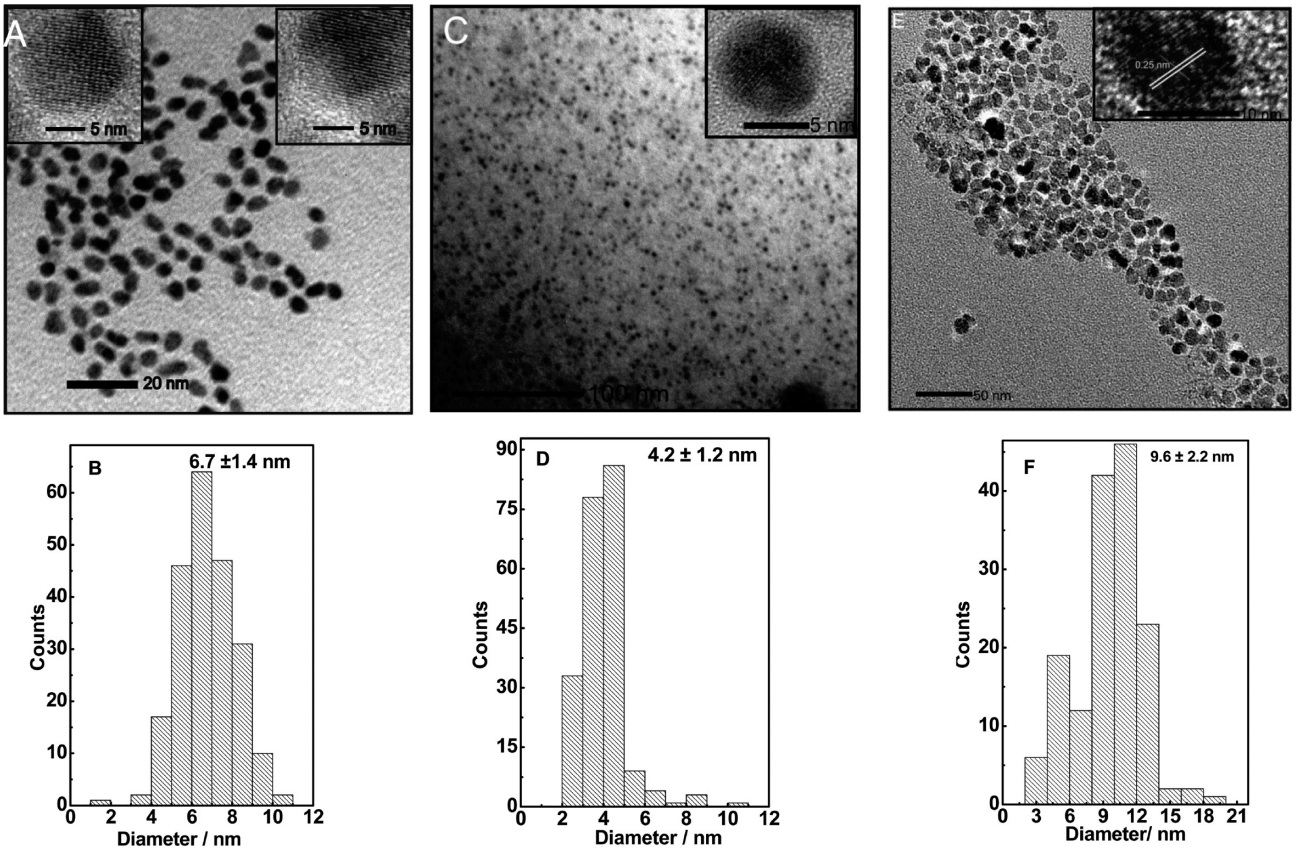

Figure 2. (A) TEM image of large Fe_3Si nanoparticles. Insets: HRTEM images of Fe_3Si nanoparticles representing $d(111)$ lattice fringes. (B) Size histogram of large Fe_3Si nanoparticles. (C) TEM image of small Fe_3Si nanoparticles. (D) Size histogram of small Fe_3Si nanoparticles. (E) TEM image of different phase (β-$FeSi_2$) nanoparticles. Insets: HRTEM images of β-$FeSi_2$ nanoparticles representing $d(222)$ lattice fringes. (F) Corresponding size histogram of the β-$FeSi_2$ nanoparticles.

pentacarbonyl and 0.28 M silicon tetrachloride that corresponds to the XRD patterns (I) in Figure 1c. Figure 2b shows the size histogram of the corresponding Fe_3Si nanoparticles.The average size of the nanoparticles is 6.7 nm with standard deviation of ± 1.4 nm. The particle distribution shows some degree of polydispersity revealing the inhomogeneous nucleation of silicon and iron nanoparticles (note: silicon precursor is injected in the second step). Within the resolution of the low-resolution TEM, the image reveals irregularly shaped, multifaceted nanocrystals with sharp edges. Figure 2a insets show the high resolution transmission electron microscope (HRTEM) images of large Fe_3Si nanoparticles and the material is highly crystalline with clearly seen lattice fringes. Insets show the $d(111)$ lattice fringes of $D0_3$ cubic structure with lattice spacing 0.32 nm. The experimental results of the lattice spacing from HRTEM are similar to that of $d(111)$ lattice spacing obtained from XRD (Figure 1a) and confirms the crystalline nature and the formation of Fe_3Si nanoparticles. The calculated $d(111)$ spacing for the bulk Fe_3Si is 0.32 ± 0.01 nm.

The size-controlled growth of the nanoparticles is crucial to producing well-defined iron silicide nanoparticles; here the size of the nanoparticles depends on the ratios of the precursor molecules. Changing the concentration of reacting precursor molecules at fixed molar ratios of 3:1 for iron to silicon produces the Fe_3Si nanoparticles of different sizes. Figure 2c represents the small Fe_3Si nanoparticles prepared by using 0.15 M of silicon tetrachloride and 0.46 M of iron pentacarbonyl. The nanoparticles in this case are nearly monodisperse with average size of 4.2 nm and standard deviation of ± 1.2 nm (Figure 2d). The inset shows the HRTEM of the same nanoparticles, revealing that nanoparticles are amorphous in this particular composition. This result is consistent with the XRD results shown in Figure 1c (III). When the precursors molar ratio for iron to silicon are changed to 1:2, the reaction forms the β-$FeSi_2$ nanoparticles previously shown in Figure 1d (I). The average

(25) Li, W.; Ni, C.; Lin, H.; Huang, C. P.; Shah, S. I. *J. Appl. Phys.* **2004**, *96*(11), 6663–6668.
(26) Jinlian, H.; Weiping, C.; Cuncheng, L.; Yanjie, G.; Li, C. *Appl. Phys. Lett.* **2005**, *86*(15), 151915.
(27) Klemmer, T. J.; Shukla, N.; Liu, C.; Wu, X. W.; Svedberg, E. B.; Mryasov, O.; Chantrell, R. W.; Weller, D.; Tanase, M.; Laughlin, D. E. *Appl. Phys. Lett.* **2002**, *81*(12), 2220–2222.
(28) Hunt, T. D.; Reeson, K. J.; Homewood, K. P.; Teon, S. W.; Gwilliam, R. M.; Sealy, B. J. *Nucl. Instrum. Method Phys. Res., Sect. B* **1994**, *84*(2), 168–171.
(29) Hunt, T. D.; Sealy, B. J.; Reeson, K. J.; Gwilliam, R. M.; Homewood, K. P.; Wilson, R. J.; Meekison, C. D.; Booker, G. R. *Nucl. Instrum. Methods Phys. Res., Sect. B* **1993**, *74*(1−2), 60–64.
(30) Udono, H.; Kikuma, I.; Okuno, T.; Masumoto, Y.; Tajima, H.; Komuro, S. *Thin Solid Films* **2004**, *461*(1), 182–187.
(31) Yoshitake, T.; Yatabe, M.; Itakura, M.; Kuwano, N.; Tomokiyo, Y.; Nagayama, K. *Appl. Phys. Lett.* **2003**, *83*(15), 3057–3059.
(32) Oostra, D. J.; Bullelieuwma, C. W. T.; Vandenhoudt, D. E. W.; Felten, F.; Jans, J. C. *J. Appl. Phys.* **1993**, *74*(7), 4347–4353.

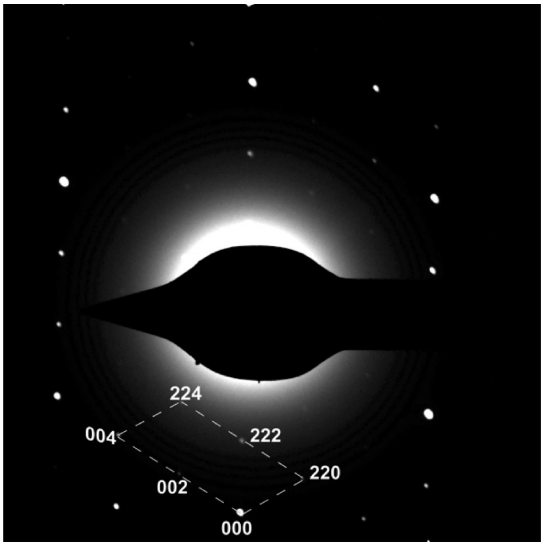

Figure 3. Electron diffraction patterns of the large Fe_3Si nanoparticles. The zone axis is parallel to $(1\bar{1}0)$ direction.

size and morphology of the particles is represented by the TEM image as shown in Figure 2e. The TEM image shows that the β-$FeSi_2$ nanoparticles are not spherical and larger than Fe_3Si nanoparticles. The sudden change in size and morphology is probably due to deposition selectivity of precursor molecules during the growth of nanoparticles. Figure 2f shows the histogram of the corresponding β-$FeSi_2$ nanoparticles and the average size is 9.6 nm with standard deviation of 2.2 nm. The inset shows the HRTEM image of β-$FeSi_2$ nanoparticles where the lattice fringes are clearly seen. The value of lattice spacing measure from HRTEM is 0.24 nm corresponds to $d(222)$ lattice. The calculated bulk value of $d(222)$ lattice of β-$FeSi_2$ is 0.24 nm $\pm$0.01 nm. The result implies that particles are growing continuously without phase segregation of the elements and are single-crystalline.

Further characterization of the nanoparticles is performed by using electron diffraction associated with HRTEM. The diffraction spots are obtained by focusing the electrons beam on single particle and the spots are simulated by using ratiometric and vector addition method.[33] For the spots identification, zone axis is considered parallel to the $(1\bar{1}0)$ direction. All the distinct and identifiable points (Figure 3) are attributed to the crystallinity of the particles and correspond to the different lattice planes of the $D0_3$ type large Fe_3Si nanoparticles. Absence of diffraction rings confirms that the nanoparticles are neither randomly oriented like grains in polycrystalline foils nor like spheroidal particles in films. The nanoparticles are not forming the super lattice as there are no evidence of super lattice diffraction spots.[34]

Iron silicide nanoparticles are relatively hard materials that allow size distribution determination by atomic force microscopy (AFM) from the topography of the as deposited nanoparticles on flat surfaces such as Si $\langle 111 \rangle$.

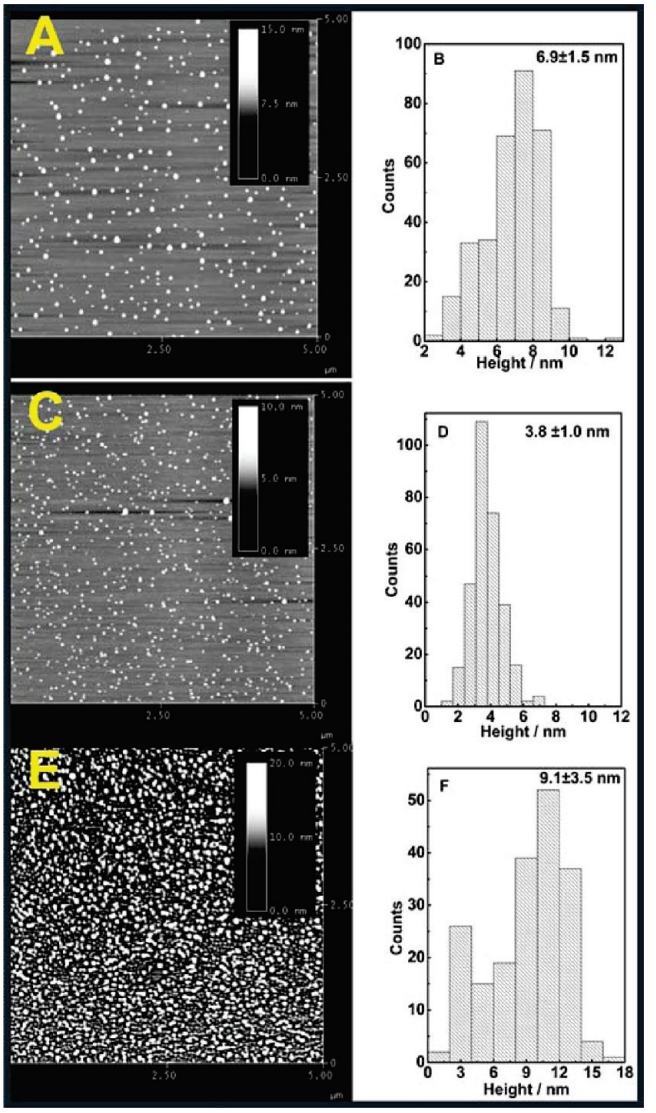

Figure 4. Tapping mode AFM images of (A) large Fe_3Si, (C) small Fe_3Si, and (E) β-$FeSi_2$ nanoparticles. (B), (D), and (F) are their corresponding height histograms.

The flatness of the Si $\langle 111 \rangle$ surface measured from tapping mode AFM is 0.2 nm. In AFM particles, size is defined by the maximum height of the particles and gives the three-dimensional projection of the nanoparticles. The deposited Fe_3Si nanoparticles on Si $\langle 111 \rangle$ are analyzed by tapping mode AFM. Banin and co-workers pointed out that nanoparticle height could be underestimated by AFM in free air because the recorded height is the sum of the topography and the force gradient contribution.[35] Therefore, to increase the visibility of the particles during analysis (not shown), the AFM images of nanoparticles on Si $\langle 111 \rangle$ are enhanced by taking the negative eigenvalues of the Hessian function of the image. The image enhancement step is followed by the selection of a 15 nm diameter circular region encompassing the visually enhanced particles. The difference between the median of the lowest 3 pixels and highest three pixels are taken as the height of the particles. This process ensures that artifacts

(33) www.matter.org.uk/diffraction/electron.
(34) Ueda, K.; Ando, Y.; Kumano, M.; Sadoh, T.; Maeda, Y.; Miyao, M. *Appl. Surf. Sci.* **2008**, *254*(19), 6215–6217.
(35) Ebenstein, Y.; Nahum, E.; Banin, U. *Nano Lett.* **2002**, *2*(9), 945–950.

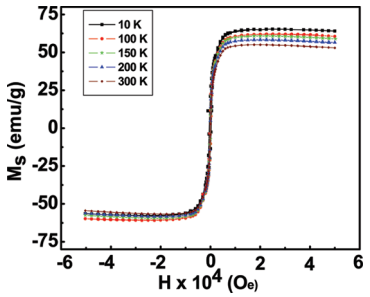

Figure 5. Magnetization vs applied magnetic field curve for Fe_3Si nanoparticles ranging from 10 to 300 K.

associated with the AFM technique (such as spikes) are minimized. The histograms of the particles are generated by adding up several hundreds of particles. The tapping mode AFM image of large Fe_3Si nanoparticles are shown in Figure 4a and corresponding average particles height is 6.9 ± 1.5 nm is represented by the histogram in Figure 4b. Figure 4c is AFM image for the small Fe_3Si nanoparticles and corresponding average height distribution is 3.8 ± 1.0 nm as shown by the histogram in Figure 4d. Similarly, Figure 4e shows the AFM image of β-$FeSi_2$ nanoparticles with average height distribution of 9.1 ± 3.5 nm (Figure 4f). The summary of the TEM, AFM, and XRD measurements are shown in Table 1.

From Table 1, it is concluded that the height measurement of the nanoparticles by using AFM is in good agreement with the TEM particle size measurement. As expected, the morphology and shape of the nanoparticles are similar in both AFM and TEM images. Composition of the nanoparticles is examined by using energy-dispersive X-ray analysis (EDX). EDX point analysis is carried out by focusing electron beam at least for seven different particles and the average composition is calculated. Figure S2a (Supporting Information) is the typical EDX spectra obtained from single large Fe_3Si nanoparticles. The spectra show approximately 3 times more intense peak for iron compare to silicon and the average composition is 0.18 ± 0.01 at % silicon and 0.56 ± 0.02 at % iron. Similarly, Figure S2b is a typical EDX spectra obtained from single $FeSi_2$ nanoparticles that are prepared by taking 1:2 molar ratio of iron to silicon precursors. The EDX spectra shows approximately 2 times intense peak of silicon to that of iron and the ratio of peak area is approximately proportional to the molar ratio of the Si to Fe. The average composition is 0.08 ± 0.01 atomic % of iron and 0.14 ± 0.01 atomic % of silicon. The overall average composition of each element is shown in the Supporting Information.

Magnetic properties of the large Fe_3Si nanoparticles are studied by using a commercial superconducting quantum interference device (SQUID) magnetometer. Figure 5 shows the magnetization curves with respect to the applied magnetic field at five different temperatures. At all temperatures, the Fe_3Si nanoparticles do not show hysteresis loops, implying that the particles are superparamagnetic. The average saturation magnetization of large Fe_3Si nanoparticles is 60 emu/g which is very similar to that of iron oxide (Fe_3O_4) nanoparticles (61 emu/g)[36] and less than iron nanoparticles, which is 171 emu/g.[37] The saturation magnetization is higher at lower temperature (10 K) and lower at higher temperature (300 K) because of increasing thermal energy that overcomes the electronic spin exchange and produces a randomizing effect.[38,39] The absence of hysteresis is attributed to the small particle size and finite size effect in the nanoparticles.[39]

Conclusion

Fe_3Si nanoparticles are prepared by a high-temperature reduction method. The particles show superparamagnetic nature at temperature 10 to 300 K as estimated from SQUID magnetometry measurements. The variation in mole ratios of reacting precursor molecules is a key to controlling the nanoparticle phase. It is believed that improvement of this work can open a road to prepare a new class of nanoparticles that is environmentally friendly, cheaper, and technologically important.

Acknowledgment. The authors are grateful to the Department of Chemistry at Kansas State University for funding. We are thankful to the University of Kansas Microscope facility. The authors also acknowledge Dr. Neeraj Nepal, Department of Electrical and Computer Engineering, North Carolina State University, for help with the magnetic properties study. This research has been made possible by Grant ACS DRF #49320-DNI10 from the American Chemical Society.

Supporting Information Available: Additional figures and data (PDF). This material is available free of charge via the Internet at http://pubs.acs.org.

(36) Lee, Y.; Lee, J.; Bae, C. J.; Park, J. G.; Noh, H. J.; Park, J. H.; Hyeon, T. *Adv. Funct. Mater.* **2005**, *15*(3), 503–509.
(37) Gong, W.; Li, H.; Zhao, Z. G.; Chen, J. C. *J. Appl. Phys.* **1991**, *69* (8), 5119–5121.
(38) Sellmyer, D., Skomski, R. *Advanced Magnetic Nanostructures*;: Springer: New York, 2006; p 507.
(39) Lu, A. H.; Salabas, E. L.; Schuth, F. *Angew. Chem., Int. Ed.* **2007**, *46*(8), 1222–1244.